# Microstructure and properties of nano-C and in-situ $Al_2O_3$ reinforced aluminum matrix composites processed by High-Pressure Torsion

Jinmei Chen[a,b], Xiaosong Jiang[a,b*], Lan Lyu[a,b], Yanjun Li[c*], Pål Christian[c], Hongliang Sun[a,b], Rui Shu[d]

[a]*Key Laboratory of Advanced Technologies of Materials, Ministry of Education, Chengdu 610031, China*

[b]*School of Materials Science and Engineering, Southwest Jiaotong University, Chengdu Sichuan 610031, China*

[c]*Department of Materials Science and Engineering, Norwegian University of Science and Technology, Trondheim 7491, Norway*

[d]*Forschungszentrum Jülich GmbHInstitut für Energie-und Klimaforschung Plasmaphysik (IEK-4) 52425 Jülich, Germany*

*Corresponding author: xsjiang@swjtu.edu.cn (X.S. Jiang), Tel./Fax: +86-28-87600779 OR yanjun.li@ntnu.no (Y.J. Li), Tel./Fax: +47 73551206.

# Microstructure and properties of nano-C and in-situ $Al_2O_3$ reinforced aluminum matrix composites processed by high-pressure torsion

In this study, Al-Si matrix composites reinforced with In situ $Al_2O_3$, C nanotubes (CNTs), and graphene nanoplatelets (GNPs) were prepared by ball milling, hot-isostatic pressing (HIP), and subsequent high-pressure torsion (HPT). Microstructures, interfacial bonding, and electrical and mechanical properties of the composites were analysed. In situ $Al_2O_3$ particles and whiskers were formed via reaction between Al powder and $SiO_2$ powder. Grains of the composites were significantly refined and reinforcements were well-dispersed in the matrix by HPT. A sub-micron equiaxed grain structure with an average grain size of 0.60 μm was obtained. Interface between the CNTs and the matrix was narrow and had no brittle phase. With an increase in the number of HPT cycles, microhardness and electrical conductivity of the composites increased. Strengthening mechanism of the Al matrix composites was mainly fine-grain strengthening. Dislocation accumulation and grain boundary evolution caused by HPT were examined.

Keywords: Al-Si matrix composites; interface; high-pressure torsion; electrical property; mechanical property; strengthening mechanism

## 1 Introduction

Al matrix nanocomposites possess high specific strength, high specific stiffness, and light weight and are widely used in the aerospace, modern transportation, and electronic fields [1, 2]. Nano-C materials, including CNTs and GNPs, are ideal reinforcements for metal materials and are extensively used to improve the mechanical and electrical properties of these materials [3-5]. GNP is a two-dimensional material with sp2 hybridization, which has excellent mechanical and physical properties, for instance, a Young's modulus of 1 TPa, a tensile strength of 130 GPa, a conductivity of $1.5 \times 10^4$ $cmV^{-2}$, and a thermal conductivity of $3 \times 10^3$ $W(m•K)^{-1}$ [3, 4]. CNTs have a unique tubular structure with a high elastic modulus and tensile strength of 1 TPa and 30 GPa, respectively [5].

However, owing to their large van der Waals forces, GNPs and CNTs easily agglomerate [6, 7]. To improve the dispersion of nano-C in the matrix and enhance its binding to the matrix material, presently, the following methods are mainly used: (1) In situ method [8-10]: He et al. [10] used an in situ method to generate CNTs in Al powder, which increased the interfacial bonding force between CNTs and Al powder. (2) Medium method [11, 12]: a medium is added or generated such that it tightly combines with both nano-C and the matrix. (3) Surface modification [13, 14], including ultrasonic treatment of CNTs in an acidic mixture ($H_2SO_4$:$HNO_3$ = 3:1), which improves the dispersion of CNTs in the matrix [9, 14].

Methods for the preparation of metal matrix composites primarily comprise liquid-and solid-state syntheses. However, the density of nano-C is quite different from that of the Al matrix; thus, the liquid-state synthesis easily causes the agglomeration of nano-C, resulting in microcracks and hole [15]. Solid-state preparation mainly adopts powder metallurgy methods, including conventional sintering [16, 17], spark plasma sintering [18, 19], hot pressing [20, 21], and hot extrusion [22-24]. These methods require high temperatures, which lead to grain coarsening and deteriorate the properties of the material.

High-pressure torsion (HPT) is one of the most commonly used severe plastic deformation technologies. The large deformation strain produced by HPT can significantly refine the grains of metals and alloys down to nanoscale [25, 26]. When HPT was applied to fabricate metal matrix composite materials, it also promoted the dispersion of reinforcements in the matrix and their binding to the matrix materials. Huang et al. [15] demonstrated that the high shear strain of HPT disintegrated the agglomerated GNPs in the Al matrix, overcame the problem of low wettability between GNPs and the Al matrix, and dispersed the reinforcements in the matrix.

Al matrix composites synergistically reinforced by nano-C and $Al_2O_3$ have shown excellent properties as reported in our previous study [27]. Nevertheless, the agglomeration of

nano-C and its inadequate interfacial bonding with the metal matrix limit the preparation and application of these composites [27]. Herein, surface-modified GNPs, CNTs, and in situ $Al_2O_3$ were used as reinforcements to prepare Al-Si matrix composites by hot-isostatic pressing (HIP). The as-prepared composites were further processed by HPT. Microstructures of the composites were systematically characterised, their hardness and electrical properties were measured, and interfacial bonding and strengthening mechanisms were comprehensively discussed based on the experimental results.

## 2 Materials and methods

### *2.1 Materials and preparation*

In this study, Al matrix composites separately reinforced with 1.0%CNT, 0.5%GNP, 0.75%CNT+0.25%GNP, and hybrid $Al_2O_3$ were fabricated, the detailed process of which is reported in a previous study [27]. Al powder (diameter: 26-30 μm, XFNANO China), $SiO_2$ powder (diameter: 13 μm, XFNANO China), CNTs (diameter: 20-30 nm, length: 10-30 μm, XFNANO China), and GNPs (⩽10 layers, XFNANO China) were used as raw materials. In situ $Al_2O_3$ was synthesised by reacting $SiO_2$ powder with Al powder, as shown in formula (1). Gallic acid and rutin were employed to modify the CNTs and GNPs respectively. Powdered raw materials were mechanically alloyed using a planetary ball mill (WL-1, DECO). The ball-milled slurry was vacuum freeze-dried (FD-A-50, Biocool). The composite powder was pre-densified using a cold isostatic pressing machine (KJY c200, Shanxi Jinkaiyuan Industrial Co., Ltd, China). Sintering of the powders was performed in a HIP furnace (QIH-15, ABB USA) at 800 ℃ under a pressure of 70 MPa for 0.5 h [27].

$$(4+m)Al + 3SiO_2 = 2Al_2O_3 + 3Si + mAl \quad (1)$$

To reduce the grain size of the sintered specimens, disintegrate the nano-C aggregates, and improve the dispersion of reinforcements in the matrix [28], HPT was used to further process the as-prepared composites. HPT machine (MTS 311) employed herein comprised an HPT-4 system of the MTS. The maximum pressure and torque were 200 tons and 1.5 Nm, respectively. Disc-shaped HPT specimens with a diameter of 10 mm and a height of 1.5 mm were transversely cut from the Al matrix composite ingots after HIP. The specimens were consolidated by HPT at 6 GPa and room temperature, and the rotational speeds were 0.5, 2, and 5 rpm (HPT 0.5, 2, and 5 N), respectively. The preparation process of the composites is shown in Figure 1.

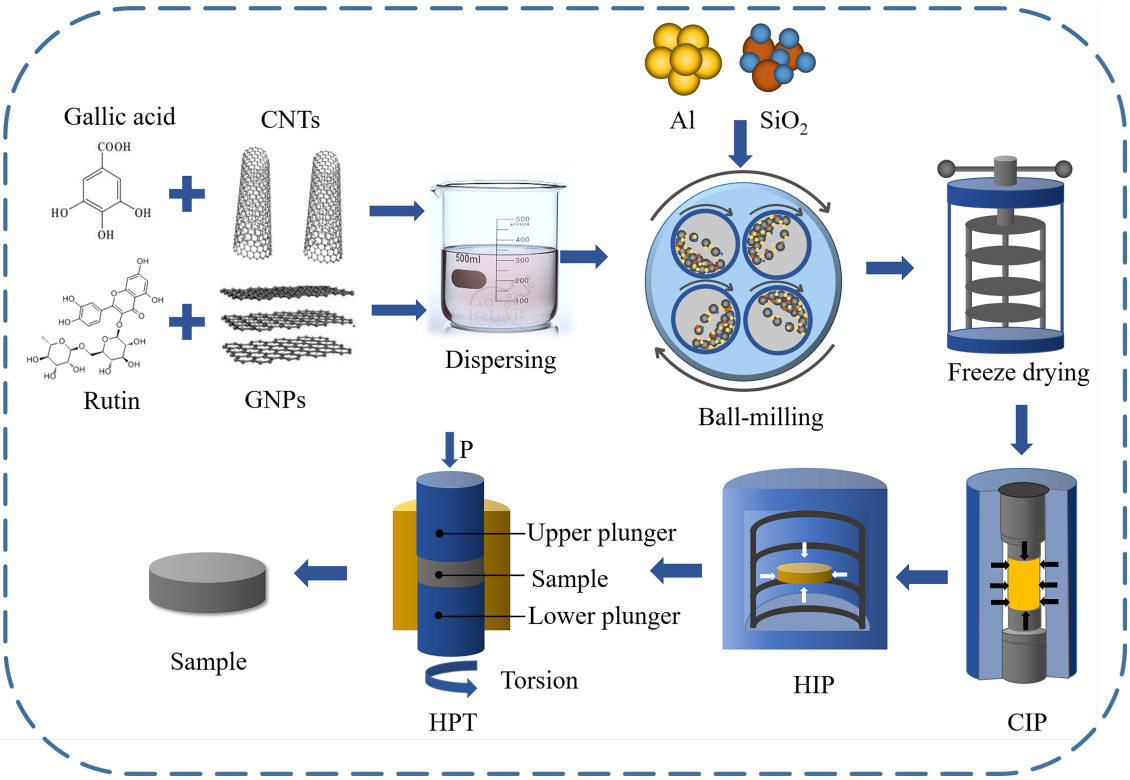


Figure 1. Schematic of the preparation of Al-Si-$Al_2O_3$-nano-C composites

### *2.2 Characterisation*

Phases of the Al-Si-$Al_2O_3$-nano-C composites during different HPT cycles were analysed by X-ray diffraction (XRD, Panalytical X'Pert Pro-MPD). Microstructures and chemical

compositions of the composites were studied by scanning electron microscopy (SEM, JEOL JSM-7001F). Grain orientations, grain sizes, and misorientation angles of the grain boundaries of the composites were examined by electron backscattering diffraction (EBSD, Oxford NordlysMax3). Microstructures of the HPT-treated Al matrix composites were further studied by transmission electron microscopy (TEM, JEOL JM-2100F). Resistivities of the composites were evaluated by a conductivity tester (Foerster Sigmatest 2.069). A microhardness tester (HXD-1000TM, Shanghai Optical Instrument Co., Ltd) was employed to measure the hardness of the HPT-treated composites at different positions of the cross section.

## 3 Results

### *3.1 Material phase analysis*

Figure 2 shows the XRD patterns of the Al-Si-$Al_2O_3$-1.0%CNT composite achieved after different HPT cycles. The composite is mainly composed of an Al-Si matrix and small amounts of γ-$Al_2O_3$ and $Al_4C_3$. There was no new phase in the composite after HPT treatment, only the peak strength changed. No diffraction peaks of CNTs were detected because C is a light element and is present in low concentration. The diffraction peak of $SiO_2$ was also not observed, indicating that the in situ reaction between $SiO_2$ and Al powders was completed. Moreover, a small amount of $Al_4C_3$ was found in the composite. The transition-state C on the surface of CNTs reacted with the Al matrix during HIP [29] as follows:

$$4Al + 3C = Al_4C_3 \ , \ \Delta G = -266520 + 92.3T \qquad (2)$$

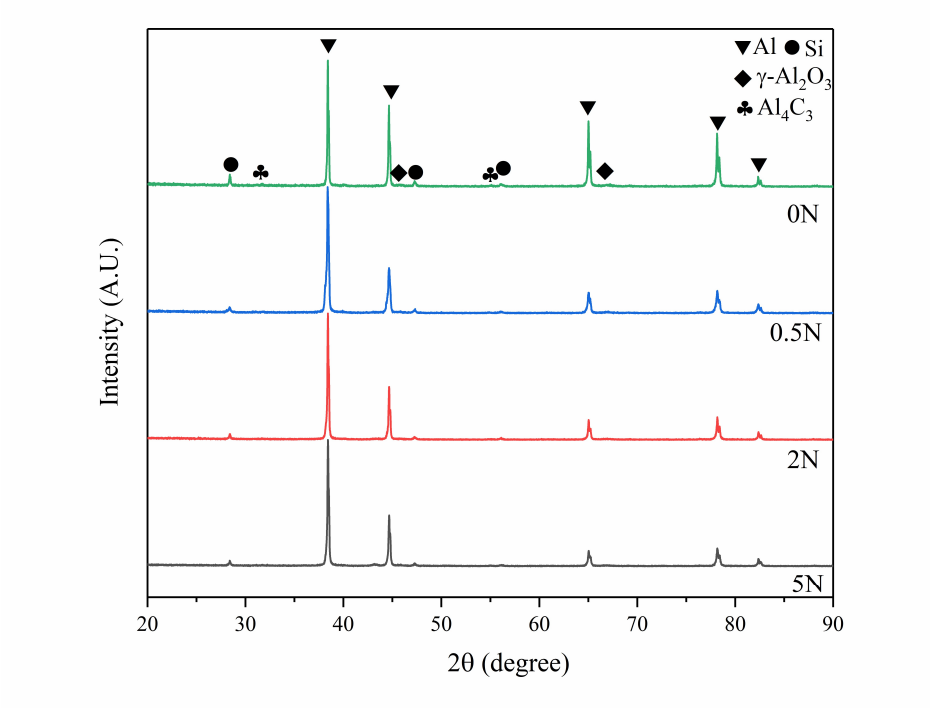


Figure 2. XRD patterns of the Al-Si-$Al_2O_3$-1.0%CNT composites obtained after different cycles of HPT

### *3.2 Microstructure and interface analysis*

SEM images of the Al-Si-$Al_2O_3$-1.0%CNT composites are shown in Figure 3. The Al-Si alloy matrix shows a grey contrast. Due to the high content of C at point 2, it was concluded that the pits were generated by the falling off of the CNT aggregates during polishing. The sizes of the pits decreased with an increase in the number of HPT cycles, which implied that the agglomeration of CNTs decreased. This was because the shear strain and turbulence produced by HPT broke the CNT aggregates and improved the dispersion of CNTs in the matrix. The existence of local turbulence has been demonstrated in duplex stainless steel [30, 31] and Al matrix composites [32] fabricated by HPT. Furthermore, the white particles at point 3 were determined to be $Al_2O_3$ according to the EDS results.

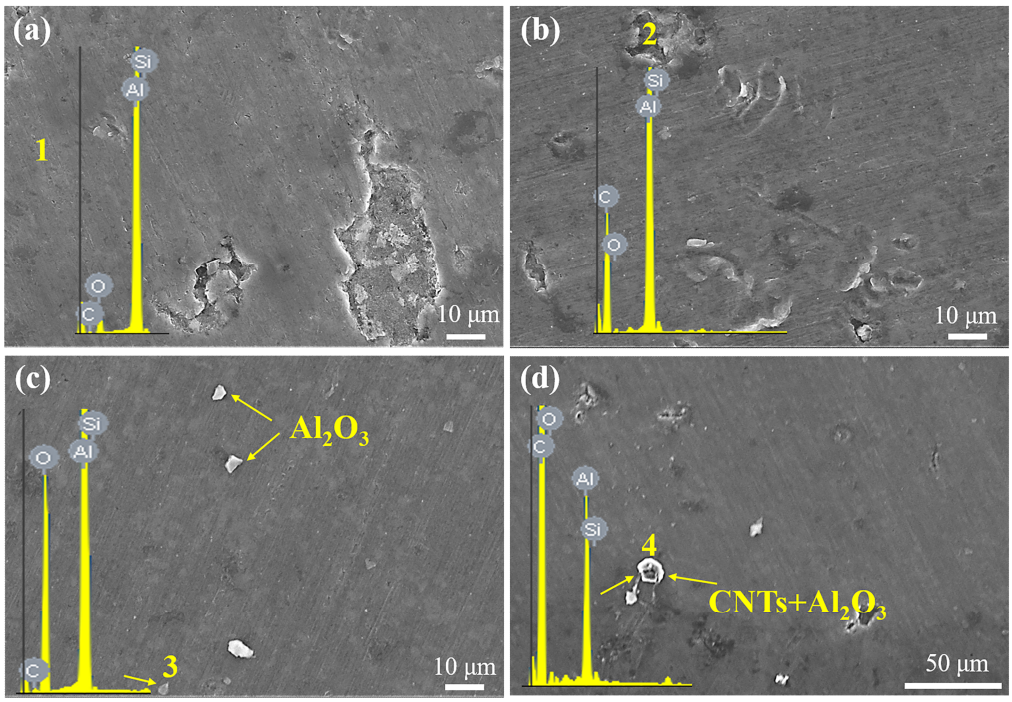


Figure 3. SEM and EDS images of the Al-Si-$Al_2O_3$-1.0%CNT composites obtained after different cycles of HPT: (a) 0, (b) 0.5, (c) 2, and (d) 5 N

Figure 4 shows the EBSD results obtained for the edge position of the Al-Si-$Al_2O_3$-0.75%CNT+0.25%GNP composite processed by HPT 5 N. The matrix has an ultrafine equiaxed grain structure with uniform grain size (Figure 4(a)). Figure 4(b) indicates that phase 1 comprises $Al_2O_3$ particles. There are white fragments on the matrix, and their distribution location is consistent with that of phase 2 in Figure 4(a). Residual stress in the black phase 2 is large, and stress is concentrated. According to the morphology and composition analysis, phase 2 is composed of nano-C, which are distributed along the grain boundary of the matrix.

Grain orientation of the composite was random (Figure 4(c)). There was no clear preferred orientation, and the microstructure distribution was uniform. The sizes of different grains (>2°) were calculated (Figure 4(d)), and the average grain size of the composite was 0.6 μm, which was smaller than those of the Al matrix composites prepared by other methods [22, 33, 34]. Therefore, the composite fabricated herein exhibited significant grain refinement

after HPT. Figure 4(e) shows the distribution of small-angle grain boundaries (LAGBs) and large-angle grain boundaries (HAGBs). LAGBs were distributed around the HAGBs. Figure 4(f) depicts a histogram of the grain boundaries, where the LAGBs account for 42.7%. The presence of a large number of LAGBs can improve the toughness of the composites because the difference between the orientations of adjacent grains is small, which can reduce the resistance of dislocation motion, and dislocations can more easily pass through the grains [35].

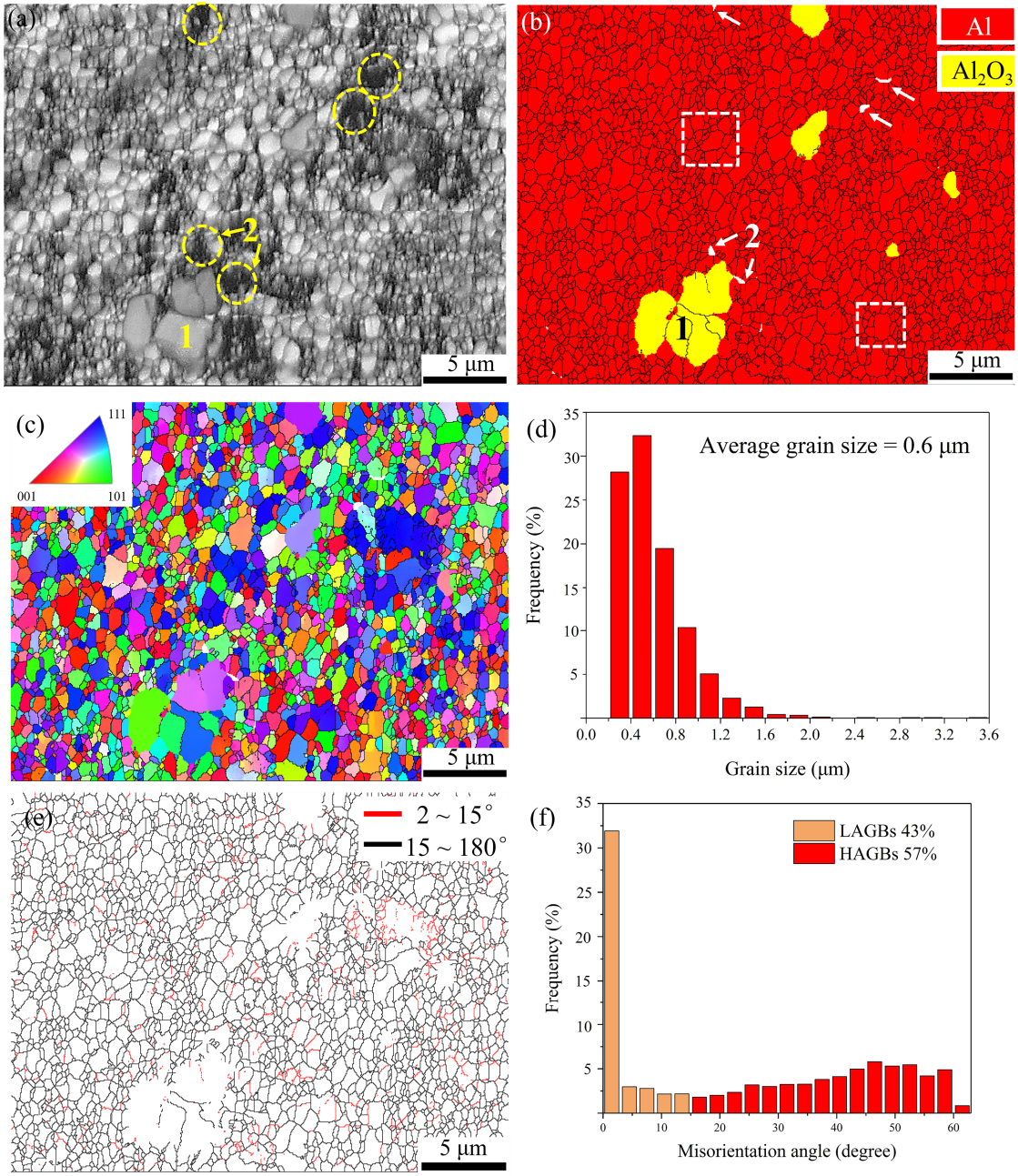


Figure 4. EBSD results achieved for the edge position of the Al-Si-$Al_2O_3$-0.75%CNT+0.25%GNP composite treated by HPT 5 N, (a) band contrast image, (b) phase hue image, (c) inverse pole figure, (d) histogram of grain size, (e) grain boundary image, and (f) histogram of the misorientation angles of grain boundaries

Figure 5 shows the TEM images of the Al-Si-$Al_2O_3$-0.75%CNT+0.25%GNP composite treated by HPT 5 N. $Al_2O_3$ is distributed at the grain boundary of Al (Figure 5(a)). Figure 5(b) shows a block-shaped particle of approximately 1 μm in size. Indexing of the SAED pattern confirmed that this particle was a single-crystal γ-$Al_2O_3$ particle formed in situ reaction. To characterise the structure of the interface between $Al_2O_3$ particles and Al matrix, a magnified image of the boxed area in Figure 5(b) is shown in Figure 5(c). The interface was rather clean without any voids or inclusions, indicating that the in situ method improved the interfacial adhesion between $Al_2O_3$ particles and Al matrix.

Large number of interlaced fibrous substances can be observed in Figure 5(d). Figure 5(e) depicts a magnified image of the block area shown in Figure 5(d), and the EDS results demonstrate that the fibrous material is $Al_2O_3$. The length and diameter of the fibres were approximately 200 and 15 nm, respectively, which indicate that the fibre was an $Al_2O_3$ whisker. Qu et al. [36] synthesised Al matrix composites reinforced with in situ $Al_2O_3$ whiskers. The whisker diameter was approximately 20 nm, and the aspect ratio was 10-15, which are similar to the results reported herein. As shown in Figure 5(d) and (e), the surface of the $Al_2O_3$ whisker is smooth without bending and breakage, which suggests that HPT does not break the structural integrity of the whisker. Figure 5(f) shows a high-resolution image of the boxed area depicted in Figure 5(e), indicating that the interface between $Al_2O_3$ and Al matrix is narrow and clean, proving the superiority of the in situ reinforcements.

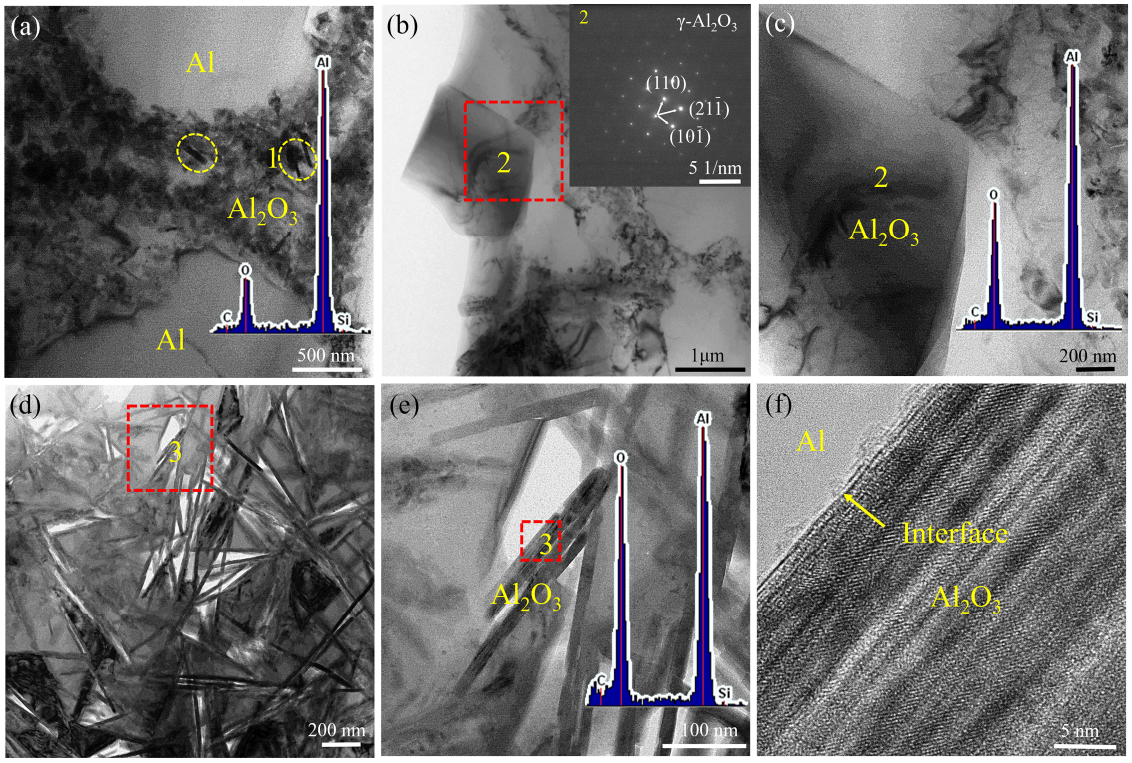


Figure 5. TEM images of the Al-Si-$Al_2O_3$-0.75%CNT+0.25%GNP composite treated by HPT 5 N

Figure 6 shows the distribution and microstructure of CNTs in the composite processed by HPT 5 N. Large number of nano-C aggregates are distributed at the grain boundaries of the Al matrix (Figure 6(a)). EDS results show that the light grey phase is mainly nano-C (Figure 6(b)). Figure 6(c) presents that CNTs have a root-like structure, which is translucent, with flake GNPs attached to the surface of CNTs. SAED pattern further proves that the phase is CNTs (Figure 6(d)). Because of the agglomeration of the CNTs and GNPs, the diffraction pattern shows concentric rings. Figure 6(e) shows a high-resolution TEM image. The planar spacing of the lattice fringe of {111}Al was 0.23 nm, and the layer spacing of CNTs was 0.35 nm, which was consistent with the findings of previous studies [26, 37, 38]. The interface between the CNTs and the matrix was narrow, with close bonding and no brittle phase.

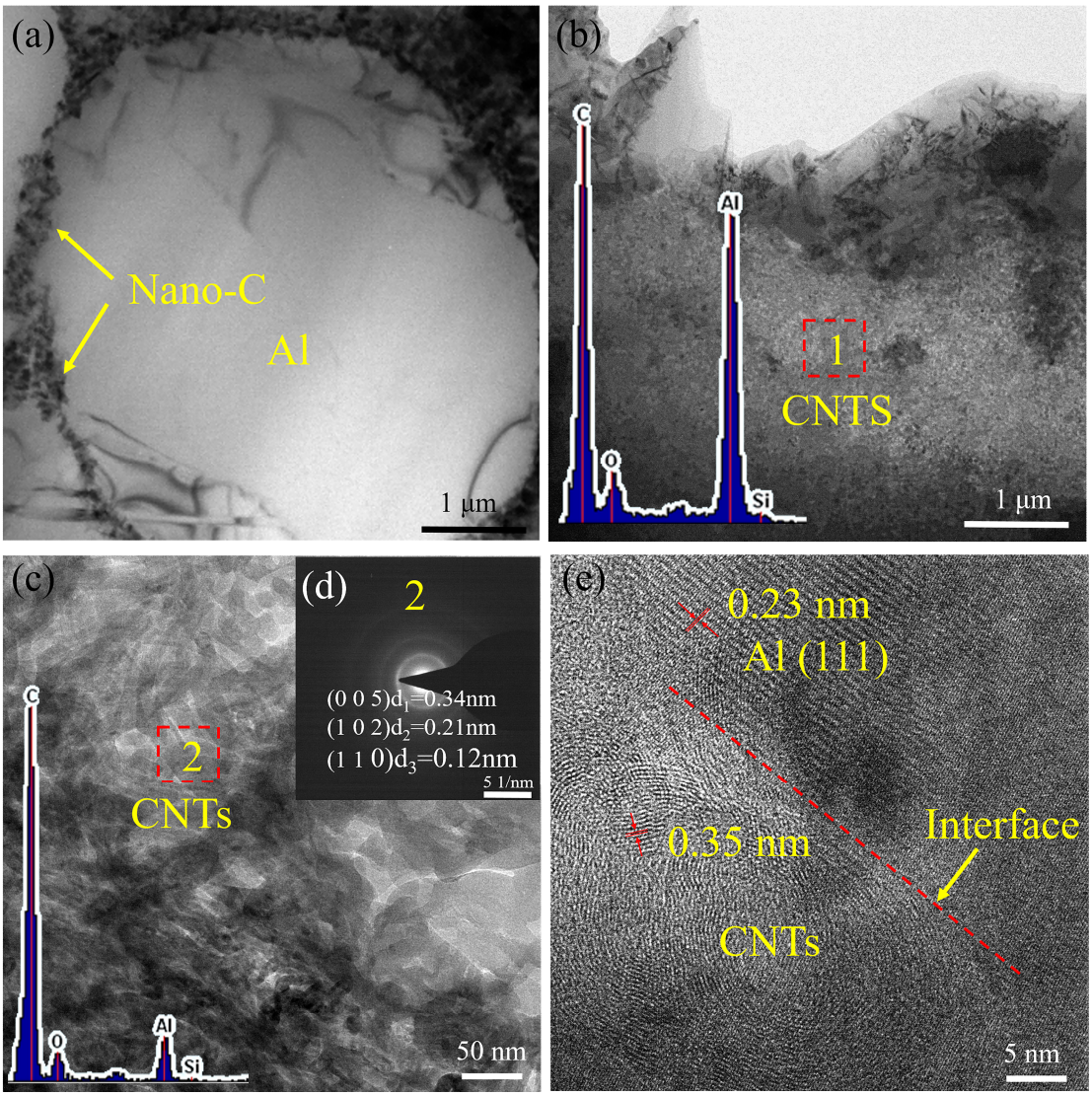


Figure 6. TEM images of nano-C in the Al-Si-$Al_2O_3$-0.75%CNT+0.25%GNP composite treated by HPT 5 N

### *3.3 Analysis of the mechanical and electrical properties*

Figure 7 shows the evolution of the resistivity of composites with different HPT cycles. The resistivity of the composites decreased with an increase in the number of HPT cycles. After HPT, the wettability between nano-C and Al significantly improved, and dislocations, voids, and microcracks at the grain boundary of the composite substantially reduced, the density

increased, and the path of electronic circulation became smoother. Moreover, the uniform structure reduced the electron scattering effect, lengthened the average free path of electrons, and improved the conductivity. The resistivity of the Al-Si-$Al_2O_3$-1.0%CNT composites was the highest, whereas that of the Al-Si-$Al_2O_3$-0.5%GNP composites was the lowest, that is, $4.18 \times 10^{-8}$ Ω m after HPT 5 N. The excellent electrical properties of CNTs were evident only along the axial direction. In contrast, as GNPs have a two-dimensional structure with high electron mobility, extremely low electron scattering rate, and excellent electrical properties [4].

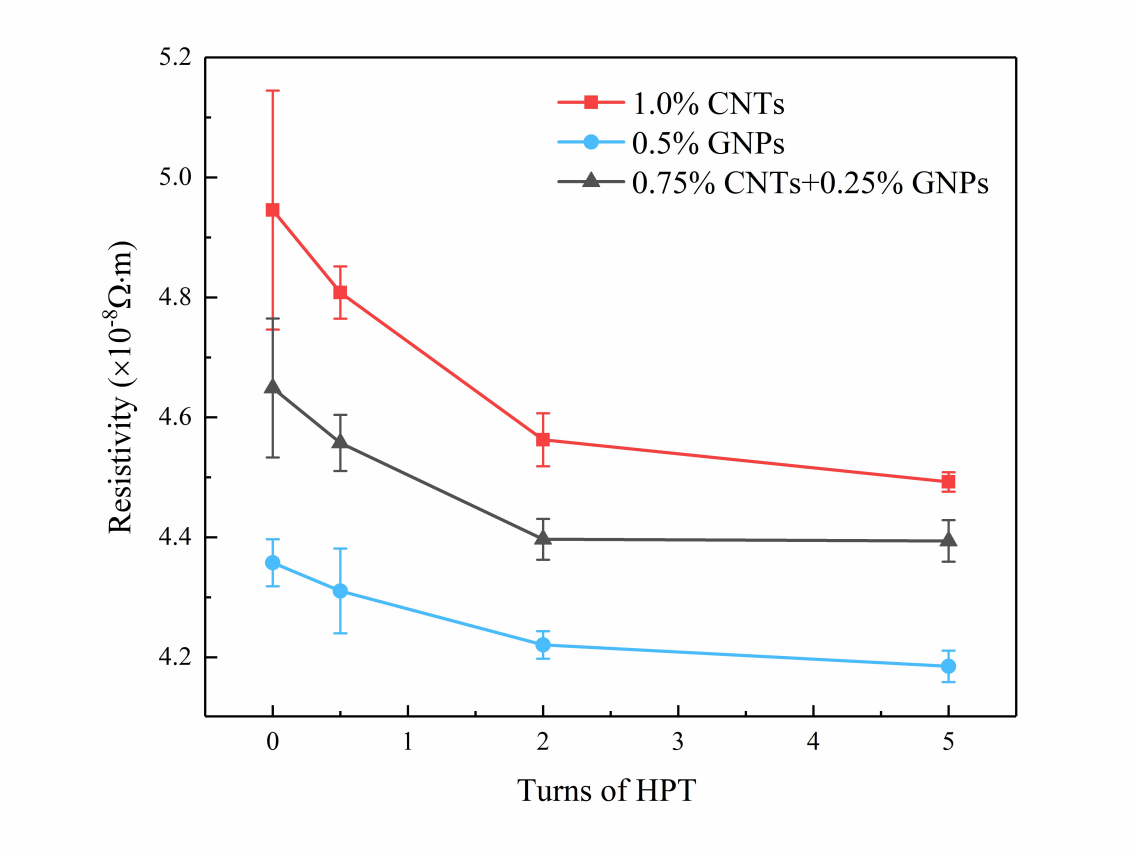


Figure 7. Variation in the resistivity of the composites with different HPT cycles

Figure 8 shows the microhardness distribution of the Al-Si-$Al_2O_3$-1.0%CNT composites after HPT 0 N, 0.5 N, 2 N, and 5 N. The microhardness distribution of the composite after HPT was very uneven; that is, the hardness at the edge was the largest,

whereas that at the centre was the smallest. This is similar to the findings reported in other studies [26, 39]. Because the shear strain at the centre was small during HPT and was large at the edge. The more the number of HPT cycles, the stronger the shear effect. Matrix grains were broken and recrystallized, and the grain size decreased, causing fine-grain strengthening. Simultaneously, the CNTs were more evenly dispersed in the matrix, which hindered the movement of dislocations.

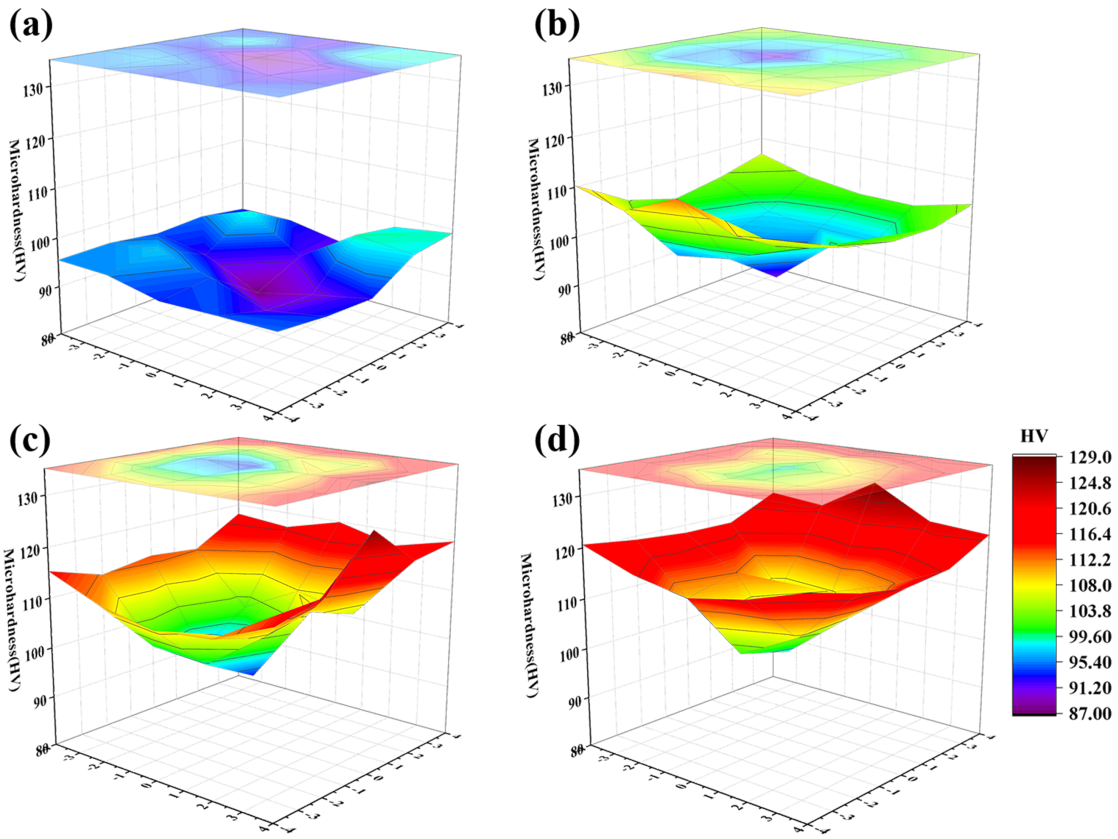


Figure 8. Microhardness of the Al-Si-$Al_2O_3$-1.0%CNT composites with variation in the distance from centre: (a) HPT 0 N, (b) HPT 0.5 N, (c) HPT 2 N, and (d) HPT 5 N

Figure 9 shows the microhardness of the Al-Si-$Al_2O_3$-0.75%CNT+0.25%GNP composites. The difference between the hardness values of the core and the edge of the composite after HPT 5 N was still very large because nano-C acted as a lubricant and

hindered stress-strain conduction. Furthermore, the difference between the hardness values of the composite after HPT 2 N and HPT 5 N was very small. This is because a certain deformation strain level is reached during HPT, dislocation absorption and dislocation proliferation attain equilibrium, forming a stable state [40].

Additionally, average hardness values of the as-prepared composites reinforced by 1.0%CNT, 0.5%GNP, and 0.75%CNT+0.25%GNP were 94.8, 87.8, and 77.5 HV, respectively. Aqeel et al. [41] suggested that the hardness of Al-Si-0.5%CNT composite obtained by HIP was approximately 58 HV, and Yazdani et al. [42] prepared a CNT- and GNP-reinforced Al matrix composite by hot pressing sintering, and the hardness was approximately 37 HV, which were lower than that of the composites fabricated herein. The preparation method and strengthening effect of the reinforcement were better in this study.

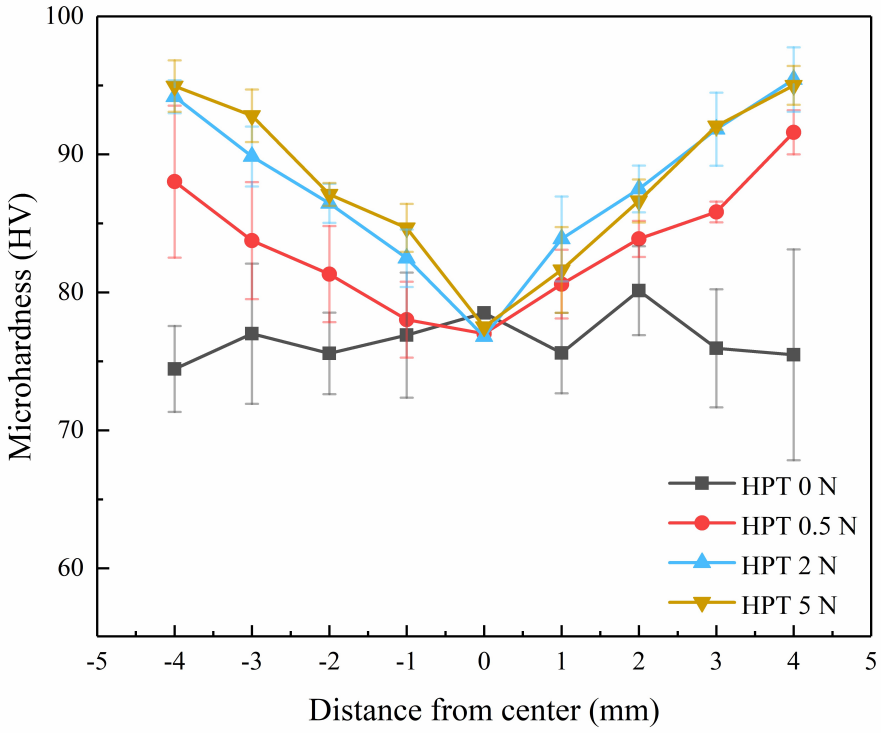

Figure 9. Microhardness of the Al-Si-$Al_2O_3$-0.75%CNT+0.25%GNP composites as a function of the distance from centre

## 4 Discussion

### *4.1 Influence of interface characteristics on the performance of composite*

As mentioned above, the hardness of the as-prepared Al matrix composites prepared herein was higher than those of the composites reported in previous studies [41, 42], which was related to the improved interfacial wetting between the reinforcements and the matrix. The in situ-synthesised $Al_2O_3$ particles and whiskers were closely bound to the matrix without any interstice or inclusions at the interface (Figure 5), which significantly increased the resistance to the initiation and propagation of cracks along the interfaces. The interface between nano-C and Al matrix was clean and free of impurities (Figure 6).

Generally, Al and nano-C easily produce $Al_4C_3$ at the interface during sintering at high temperatures [29, 43]. Herein, the XRD pattern of $Al_4C_3$ demonstrated the diffraction peak of $Al_4C_3$, and Shu et al. [27] also observed the formation of $Al_4C_3$ on the CNTs of Al matrix composites without HPT. However, the TEM results obtained in this study indicated the absence of $Al_4C_3$ at the interface between nano-C and the matrix, which was attributed to HPT. For a better understanding, a schematic of $Al_4C_3$ evolution is shown in Figure 10.

A transition carbon layer was formed on the surface of the CNTs during ball milling, and the free C atoms and Al matrix diffused to form a transition layer (Figure 10(a)). During HIP, Al reacted with free C, and continuous $Al_4C_3$ layers were produced on the surface of the CNTs (Figure 10(b)). The integrity of the $Al_4C_3$ layer was lost owing to the large strain produced during HPT (Figure 10(c)). With an increase in the number of HPT cycles, the strain increased, and $Al_4C_3$ was broken and dispersed in the matrix (Figure 10(d)). $Al_4C_3$ is a

brittle phase, and HPT results in a cleaner interface, promotes interfacial bonding, and is beneficial to the mechanical properties of the composite.

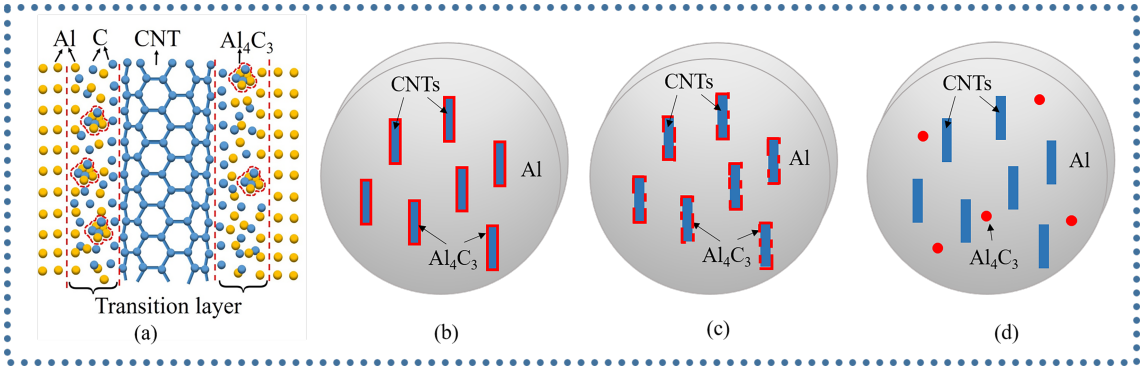


Figure 10. Schematic of interface structure and $Al_4C_3$ evolution

### *4.2 Strengthening mechanism*

Hardness of the as-prepared composite was 76 HV (Figure 9), which was substantially higher than those of Al-Si alloys [44]. This can be attributed to the strengthening of the composite by the reinforcements including CNTs, GNPs, $Al_2O_3$ whiskers, and $Al_2O_3$ particles. Reinforcements play the role of pinning the grain boundary migration and inhibiting the grain growth, which ensure that the grains in the composite remain fine and uniform even after high-temperature sintering [45].

After HPT, an increase as high as 20 HV was achieved in the hardness of the edge of the Al-Si-$Al_2O_3$-0.75%CNT+0.25%GNP composite. During large plastic deformation by HPT, the grains of the composite were further refined. Because of the impingement effect of reinforcements on dislocation migration and the formation of dislocation walls, causing a small difference in the orientation of grains, which promotes the formation of subgrain boundaries. The migration of subgrain boundaries and the rotation of subgrains increase the difference in the orientation of grains, which facilitates the transformation of subgrain boundaries to LAGBs and then to HAGBs, and their evolution into grain boundaries, which

subdivide coarse grains into ultrafine grains [26, 32, 37, 46]. Figure 11 shows a schematic of the grain refinement during HPT.

When a certain deformation strain level is reached during HPT, a balance between dislocation generation and dislocation annihilation (dynamic recovery) is achieved, and the hardness no longer increase [40, 47]. The hardness attained an equilibrium state in Figure 9. Therefore, the entire large plastic deformation process can be divided into three stages: strain hardening dominated by dislocation proliferation, fine grain strengthening caused by the formation and evolution of subgrain boundaries, and attainment of a stable state of equilibrium between dislocation proliferation and absorption.

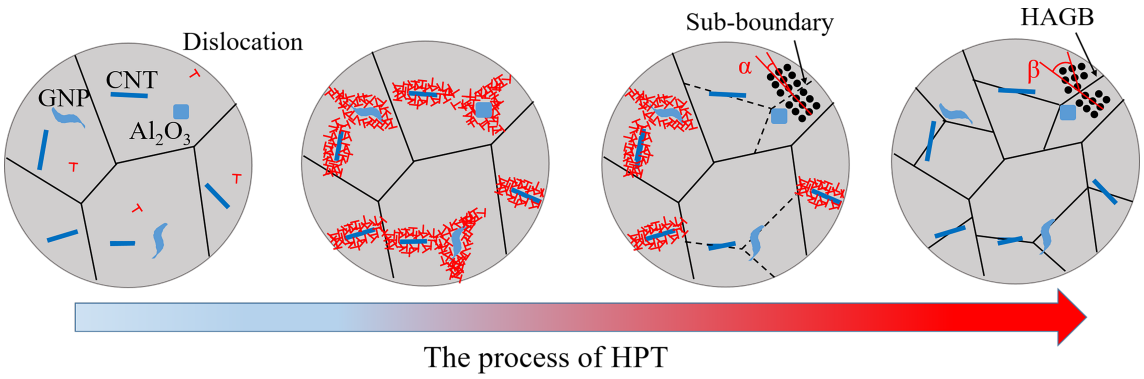


Figure 11. Schematic of grain refinement during HPT

$Al_2O_3$ particles hinder the movement of dislocations, and the dislocations cannot pass through the strong $Al_2O_3$ particles and only bend around the particles, leaving the dislocation ring, thus improving hardness of the material. CNTs can also play a role in dispersion strengthening. Chen et al. [48] reported that the reaction between CNTs and dislocations was related to their respective lengths. When the length of CNTs is less than that of the dislocation, dislocations bypass the CNTs and leave the dislocation loops. Because GNPs are two-dimensional materials, their dispersion strengthening can be ignored.

For fibre reinforcements, load transfer is an essential strengthening mechanism [49]. The $Al_2O_3$ whiskers, CNTs, and GNPs employed herein are all fibre reinforcements. The

shear lag model demonstrates that the interface bonding must be sufficiently strong to transfer the load from the matrix to the fibre through interfacial shear stress along the fibre surface during plastic deformation [50, 51]. Herein, the in situ-synthesised $Al_2O_3$ whiskers were closely bonded to the Al matrix. HPT broke the $Al_4C_3$ brittle phase produced on the surface of the CNTs and dispersed it, resulting in a clean interface between the CNTs and the matrix.

## 5 Conclusion

In this study, Al matrix composites reinforced with CNTs and GNPs at different concentrations were fabricated by powder metallurgy, and the dispersion of the reinforcements and grain refinement were improved by HPT. The results obtained herein are as follows:

(1) The higher the number of HPT cycles, the less the aggregation of nano-C. Average grain size of the HPT-treated Al-Si-$Al_2O_3$-0.75%CNT+0.25%GNP composites was 0.60 μm, and the grain orientation was randomly distributed.

(2) In situ Al2O3 particles and whiskers were simultaneously generated, and the grain size of the particles was approximately 1 μm. The interface between $Al_2O_3$ and matrix was compact. The interface between the CNTs and the matrix was narrow and had no brittle phase.

(3) Hardness values of the as-prepared Al matrix composites reinforced by 1.0%CNT, 0.5%GNP, and 0.75%CNT+0.25%GNPs were 94.8, 87.8, and 77.5 HV, respectively. With an increase in the number of HPT cycles, the microhardness and electrical conductivity of the composites increased. Hardness of the HPT-treated Al-Si-$Al_2O_3$-0.75%CNT+0.25%GNP composite remained stable.

(4) Large plastic deformation of the composites was divided into three stages: strain hardening dominated by dislocation proliferation, fine grain strengthening caused by

the formation and evolution of subgrain boundaries, and attainment of a stable state of equilibrium between dislocation proliferation and absorption. The strengthening mechanism of the composite was primarily fine-grain strengthening.

Acknowledgements

This work was supported by the Key Laboratory of Infrared Imaging Materials and Detectors, Shanghai Institute of Technical Physics, Chinese Academy of Sciences (No. IIMDKFJJ-19-08), R&D Projects Funding from the Research Council of Norway (No. 263875/H30), and the China Postdoctoral Science Foundation (Nos. 2015M570794 and 2018T110993).

Declaration of interest statement

There are no conflicts of interest.

References

1. Zhu H, Min J, Li J, et al. In situ fabrication of ($\alpha$-$Al_2O_3$+$Al_3Zr$)/Al composites in an Al–$ZrO_2$ system. Compos Sci Technol. 2010;70(15):2183-2189.
2. Rezaei MR, Shabestari SG, Razavi SH. Effect of ECAP consolidation process on the interfacial characteristics of Al-Cu-Ti metallic glass reinforced aluminum matrix composite. Compos Interfaces. 2018;25(8):669-679.
3. Lee C, Wei X, Kysar JW, et al. Measurement of the elastic properties and intrinsic strength of monolayer graphene. Science. 2008;321(5887):385-388.
4. Balandin AA, Ghosh S, Bao W, et al. Superior thermal conductivity of single-layer graphene. Nano Lett. 2008;8(3):902-907.
5. Dervishi E, Li Z, Xu Y, et al. Carbon nanotubes: synthesis, properties, and applications. Part Sci Technol. 2009;27(2):107-125.
6. Poirier D, Gauvin R, Drew RA. Structural characterization of a mechanically milled carbon nanotube/aluminum mixture. Compos Part A. 2009;40(9):1482-1489.
7. Liu X, Li J, Sha J, et al. In-situ synthesis of graphene nanosheets coated copper for preparing reinforced aluminum matrix composites. Mater Sci Eng A. 2018;709:65-71.
8. Zhou W, Yamaguchi T, Kikuchi K, et al. Effectively enhanced load transfer by interfacial reactions in multi-walled carbon nanotube reinforced Al matrix composites. Acta Mater. 2017;125:369-376.

9. He C, Zhao N, Shi C, et al. An approach to obtaining homogeneously dispersed carbon nanotubes in Al powders for preparing reinforced Al-matrix composites. Adv Mater. 2007;19(8):1128-1132.
10. Zhang X, Li S, Pan B, et al. A novel strengthening effect of in-situ nano $Al_2O_3$w on CNTs reinforced aluminum matrix nanocomposites and the matched strengthening mechanisms. J Alloys Compd. 2018;764:279-288.
11. Zhao ZY, Guan RG, Guan XH, et al. Microstructures and properties of graphene‐Cu/Al composite prepared by a novel process through clad forming and improving wettability with copper. Adv Eng Mater. 2015;17(5):663-668.
12. Zhou W, Sasaki S, Kawasaki A. Effective control of nanodefects in multiwalled carbon nanotubes by acid treatment. Carbon. 2014;78:121-129.
13. Zhou W, Yamamoto G, Fan Y, et al. In-situ characterization of interfacial shear strength in multi-walled carbon nanotube reinforced aluminum matrix composites. Carbon. 2016;106:37-47.
14. Kumar S, Singh R, Hashmi MSJ. Metal matrix composite: a methodological review. Adv Mater Process Tech. 2019;6(1):13-24.
15. Huang Y, Bazarnik P, Wan D, et al. The fabrication of graphene-reinforced Al-based nanocomposites using high-pressure torsion. Acta Mater. 2019;164:499-511.
16. Pham VT, Bui HT, Tran BT, et al. The effect of sintering temperature on the mechanical properties of a Cu/CNT nanocomposite prepared via a powder metallurgy method. Adv Nat Sci: Nanosci Nanotechnol. 2011;2(1):015006-015011.
17. Suárez S, Ramos-Moore E, Lechthaler B, et al. Grain growth analysis of multiwalled carbon nanotube-reinforced bulk Ni composites. Carbon. 2014;70:173-178.
18. Li FZ, Tian LH, Li RT, et al. Microstructure and wear resistance properties of Al/Al–Cu–Cr–Fe composites consolidated using spark plasma sintering. Compos Interfaces. 2019;27(5):515-527.
19. Guo B, Song M, Yi J, et al. Improving the mechanical properties of carbon nanotubes reinforced pure aluminum matrix composites by achieving non-equilibrium interface. Mater Des. 2017;120:56-65.
20. Jafari M, Abbasi M, Enayati M, et al. Mechanical properties of nanostructured Al2024–MWCNT composite prepared by optimized mechanical milling and hot pressing methods. Adv Powder Technol. 2012;23(2):205-210.

21. Wang AQ, Liu P, Xie JP, et al. Interface characterization, precipitate evolution, and quantitative modeling of the microstructure/strength relationship in SiCp/2024Al composite. Compos Interfaces. 2015;22(9):847-866.
22. Li J, Zhang X, Geng L. Effect of heat treatment on interfacial bonding and strengthening efficiency of graphene in GNP/Al composites. Compos Part A. 2019;121:487-498.
23. Liu X, Li J, Liu E, et al. Effectively reinforced load transfer and fracture elongation by forming $Al_4C_3$ for in-situ synthesizing carbon nanotube reinforced Al matrix composites. Mater Sci Eng A. 2018;718:182-189.
24. Salama EI, Abbas A, Esawi AMK. Preparation and properties of dual-matrix carbon nanotube-reinforced aluminum composites. Compos Part A. 2017;99:84-93.
25. Sabbaghianrad S, Langdon TG. Developing superplasticity in an aluminum matrix composite processed by high-pressure torsion. Mater Sci Eng A. 2016;655:36-43.
26. Tokunaga T, Kaneko K, Horita Z. Production of aluminum-matrix carbon nanotube composite using high pressure torsion. Mater Sci Eng A. 2008;490(1-2):300-304.
27. Shu R, Jiang X, Li J, et al. Microstructures and mechanical properties of Al-Si alloy nanocomposites hybrid reinforced with nano-carbon and in-situ $Al_2O_3$. J Alloys Compd. 2019;800:150-162.
28. Li J, Zhao G, Wu S, et al. Preparation of hybrid particulates SiCnp and $Mg_2Si$ reinforced Al-Cu matrix composites. Mater Sci Eng A. 2019;751:107-114.
29. Zhu H, Guo G, Cui T, et al. Influences of carbon additions on reaction mechanisms and tensile properties of Al-based composites synthesized in-situ by Al–$SiO_2$ powder system. Mater Sci Eng A. 2015;623:78-82.
30. Cao Y, Wang Y, Figueiredo R, et al. Three-dimensional shear-strain patterns induced by high-pressure torsion and their impact on hardness evolution. Acta Mater. 2011;59(10):3903-3914.
31. Huang Y, Kawasaki M, Langdon TG. An investigation of flow patterns and hardness distributions using different anvil alignments in high-pressure torsion. J Mater Sci. 2013;48(13):4533-4542.
32. Asgharzadeh H, Joo S-H, Kim HS. Consolidation of Carbon Nanotube Reinforced Aluminum Matrix Composites by High-Pressure Torsion. Metall Mater Trans A. 2014;45(9):4129-4137.

33. Gao X, Yue H, Guo E, et al. Preparation and tensile properties of homogeneously dispersed graphene reinforced aluminum matrix composites. Mater Des. 2016;94:54-60.
34. Van Trinh P, Van Luan N, Phuong DD, et al. Microstructure, microhardness and thermal expansion of CNT/Al composites prepared by flake powder metallurgy. Compos Part A. 2018;105:126-137.
35. Hu T, Ma K, Topping T, et al. Improving the tensile ductility and uniform elongation of high-strength ultrafine-grained Al alloys by lowering the grain boundary misorientation angle. Scripta Mater. 2014;78:25-28.
36. Qu X, Wang F, Shi C, et al. In situ synthesis of a gamma-$Al_2O_3$ whisker reinforced aluminium matrix composite by cold pressing and sintering. Mater Sci Eng A. 2018;709:223-231.
37. Zhao L, Lu H, Gao Z. Microstructure and mechanical properties of Al/graphene composite produced by high-pressure torsion. Adv Eng Mater. 2015;17(7):976-981.
38. Li M, Zhang Z, Gao H, et al. Formation of multilayer interfaces and the load transfer in graphene nanoplatelets reinforced Al matrix composites. Mater Charact. 2020;159:110018-110028.
39. Kawasaki M. Different models of hardness evolution in ultrafine-grained materials processed by high-pressure torsion. J Mater Sci. 2014;49(1):18-34.
40. Liao X, Zhao Y, Srinivasan S, et al. Deformation twinning in nanocrystalline copper at room temperature and low strain rate. Appl Phys Lett. 2004;84(4):592-594.
41. Al-Aqeeli N. Processing of CNTs reinforced Al-based nanocomposites using different consolidation techniques. J Nanomater. 2013;2013:1-10.
42. Yazdani B, Xia Y, Ahmad I, et al. Graphene and carbon nanotube (GNT)-reinforced alumina nanocomposites. J Eur Ceram Soc. 2015;35(1):179-186.
43. Wang W, Du A, Zhao X, et al. Effect of Si addition on the stability of Al-10Ti-5Cu-xSi alloy/SiC interface. Compos Interfaces. 2018;25(9):761-770.
44. Li R, Liu L, Zhang L, et al. Effect of squeeze casting on microstructure and mechanical properties of hypereutectic Al-xSi Alloys. J Mater Sci Technol. 2017;33(4):404-410.
45. Zhang H, Xu C, Xiao W, et al. Enhanced mechanical properties of Al5083 alloy with graphene nanoplates prepared by ball milling and hot extrusion. Mater Sci Eng A. 2016;658:8-15.

46. Phuong DD, Trinh PV, An NV, et al. Effects of carbon nanotube content and annealing temperature on the hardness of CNT reinforced aluminum nanocomposites processed by the high pressure torsion technique. J Alloys Compd. 2014;613:68-73.
47. Harai Y, Ito Y, Horita Z. High-pressure torsion using ring specimens. Scripta Mater. 2008;58(6):469-472.
48. Chen B, Shen J, Ye X, et al. Length effect of carbon nanotubes on the strengthening mechanisms in metal matrix composites. Acta Mater. 2017;140:317-325.
49. Kwon H, Park DH, Silvain JF, et al. Investigation of carbon nanotube reinforced aluminum matrix composite materials. Composites Sci Technol. 2010;70(3):546-550.
50. Zhang Z, Liu Z, Xiao B, et al. High efficiency dispersal and strengthening of graphene reinforced aluminum alloy composites fabricated by powder metallurgy combined with friction stir processing. Carbon. 2018;135:215-223.
51. El-Ghazaly A, Anis G, Salem HG. Effect of graphene addition on the mechanical and tribological behavior of nanostructured AA2124 self-lubricating metal matrix composite. Compos Part A. 2017;95:325-336.

Figure captions

Figure 1. Schematic of the preparation of Al-Si-$Al_2O_3$-nano-C composites

Figure 2. XRD patterns of the Al-Si-$Al_2O_3$-1.0%CNT composites obtained after different cycles of HPT

Figure 3. SEM and EDS images of the Al-Si-$Al_2O_3$-1.0%CNT composites obtained after different cycles of HPT: (a) 0, (b) 0.5, (c) 2, and (d) 5 N

Figure 4. EBSD results achieved for the edge position of the Al-Si-$Al_2O_3$-0.75%CNT+0.25%GNP composite treated by HPT 5 N, (a) band contrast image, (b) phase hue image, (c) inverse pole figure, (d) histogram of grain size, (e) grain boundary image, and (f) histogram of the misorientation angles of grain boundaries

Figure 5. TEM images of the Al-Si-$Al_2O_3$-0.75%CNT+0.25%GNP composite treated by HPT 5 N

Figure 6. TEM images of nano-C in the Al-Si-$Al_2O_3$-0.75%CNT+0.25%GNP composite treated by HPT 5 N

Figure 7. Variation in the resistivity of the composites with different HPT cycles

Figure 8. Microhardness of the Al-Si-$Al_2O_3$-1.0%CNT composites with variation in the distance from centre: (a) HPT 0 N, (b) HPT 0.5 N, (c) HPT 2 N, and (d) HPT 5 N

Figure 9. Microhardness of the Al-Si-$Al_2O_3$-0.75%CNT+0.25%GNP composites as a function of the distance from centre

Figure 10. Schematic of interface structure and $Al_4C_3$ evolution

Figure 11. Schematic of grain refinement during HPT